Appendix C

from

Silicon Microwire Photovoltaics

Thesis by
Michael David Kelzenberg

In Partial Fulfillment of the Requirements
for the Degree of
Doctor of Philosophy

California Institute of Technology
Pasadena, California

2010

(Defended May 19, 2010)

ii

Note

This appendix discusses the theory and operation of the SPCM instrument that was developed during the course of the author's PhD thesis work. It is intended to assist future users of the instrument or those preforming similar measurements elsewhere. The author's own use of the SPCM instrument and discussions of the results are presented within the main chapters of the thesis.

Appendix C

SPCM instrument

In this thesis work, instrumentation and procedures were developed for performing *scanning photocurrent microscopy* (SPCM) measurements on single Si microwire devices. This characterization technique was employed in sections 4.5 and 5.3, and was also used to characterize carrier collection in wire-array devices by Brendan Kayes and Morgan Putnam in their thesis work. [1, 2] This appendix provides details on the operation of the SPCM instrumentation.

C.1 System description

In scanning photocurrent microscopy, a localized optical excitation source is scanned (rastered) along a photovoltaic or photoconductive device. The specimen current is recorded as a function of excitation position, producing spatially resolved maps of absorption and/or carrier collection within the device. Examples of SPCM can be found in nanowire research literature. [3, 4, 5, 6, 7, 8, 9, 10, 11] This technique is also widely used in photovoltaics research (typically with lower spatial resolution), where it is often referred as a *light-beam induced current* (LBIC) technique.

Our SPCM measurements were performed using a confocal microscope with near-field scanning optical microscopy (NSOM) capabilities (WITec AlphaS-NOM), located in the Molecular Materials Research Center of the Beckman Institute at Caltech. A simplified diagram of the instrument configuration and electrical connections is shown in Figure C.1.

Optical excitation source. A variety of excitation sources can be used for SPCM, however, most measurements are performed with a $\lambda \approx 650$ nm semiconductor diode laser (<5 mW continuous) that is dedicated for use with this instrument. The laser source is mounted on a kinematic stage with micrometer adjustments for pitch and yaw. The free-space beam path consists of an optical chopper system, turning mirrors, iris diaphragms, a variable neutral density filter (NDF) wheel, and a fiber coupler. A single-mode fiber is used to couple the laser source to the microscope. The fiber coupler uses a 10× objective with a numerical aperture (N.A.) of 0.2 to focus the collimated laser source onto the optical fiber. In our work, this provided low but adequate coupling efficiencies. The free-space optics are enclosed to prevent inadvertent disruption of (or exposure to) the laser source.

1
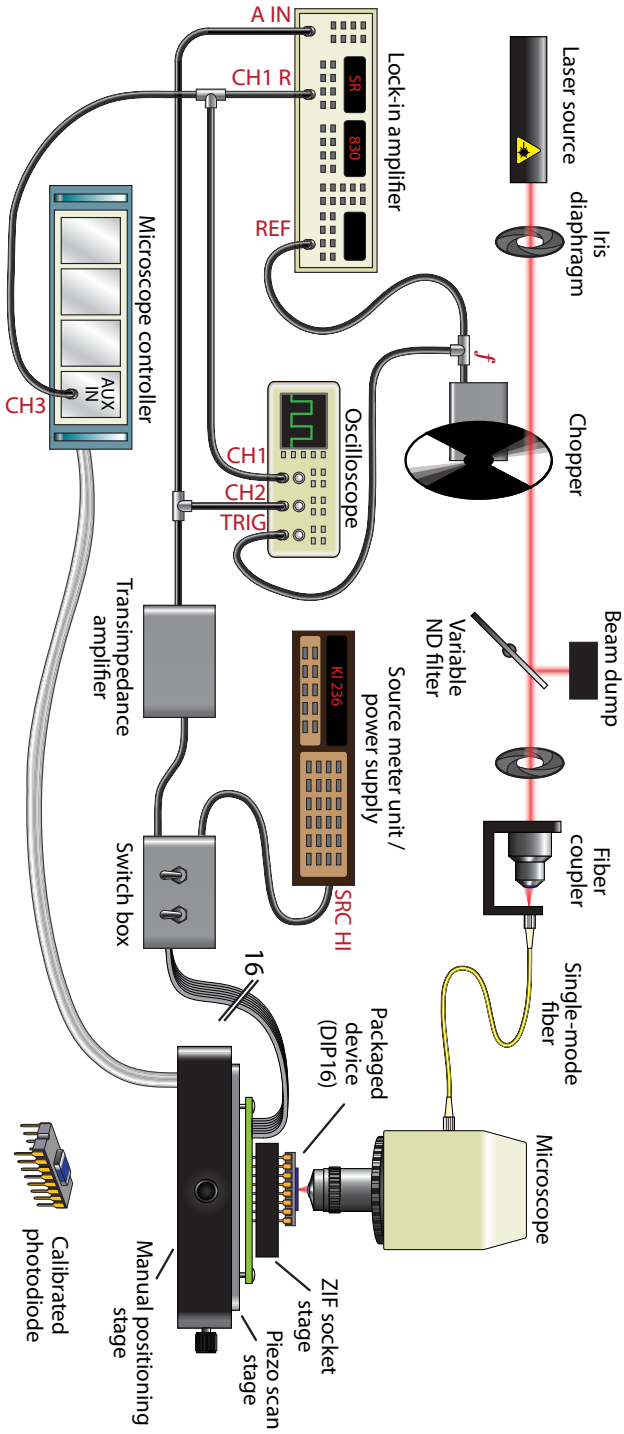
Figure C.1. Schematic illustration of SPCM instrumentation.
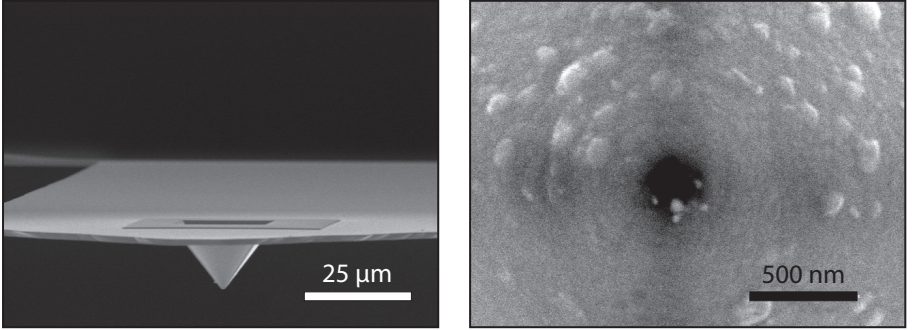
Figure C.2. Cantilevered NSOM tips. Left: side profile view. Right: aperture, enlarged to ~200 nm.

Microscope. The WITec alphaSNOM microscope system includes the microscope assembly as well as various controller modules, a support PC, and the software used to perform the experiments. Only the upper microscope optics are employed for our SPCM measurements. Broad-area illumination is provided by a variable-power halogen lamp, with condenser and field aperture diaphragms located in the upper microscope arm. Localized laser illumination is provided through an FC fiber port with an integrated focal adjustment micrometer. A 3-position beamsplitter assembly permits various combinations of broad-area and localized illumination. Reflection-mode imaging is provided by a color video camera located within the left eyepiece.

The microscope offers two excitation modes for SPCM (depicted in Fig. 4.14). For *confocal* excitation, the beam is focused to a diffraction-limited spot through the microscope objective. The minimum achievable beam waist is:

$$d_{\text{beam}} \approx \frac{0.6 \cdot \lambda}{\text{N.A.}} \tag{C.1}$$

where λ is the free-space wavelength of the light source. The highest-resolution objective available for free-space SPCM measurements in our system is presently a 50×, N.A. = 0.95 lens (larger N.A. values are possible with oil immersion).

Higher resolution can be obtained using *near-field* excitation. In this mode, a cantilevered NSOM tip is mounted at the focal point of a 10× objective, with a small aperture aligned to the excitation beam. The NSOM tip is brought into contact with the specimen and scanned using a feedback loop (similar to atomic force microscopy). New NSOM tips have nominal aperture diameters of ~90 nm. To improve the transmission of light through the tips, the apertures can be intentionally enlarged using FIB milling. Figure C.2 shows an NSOM tip whose aperture was enlarged to ~200 nm in the course of this thesis work.
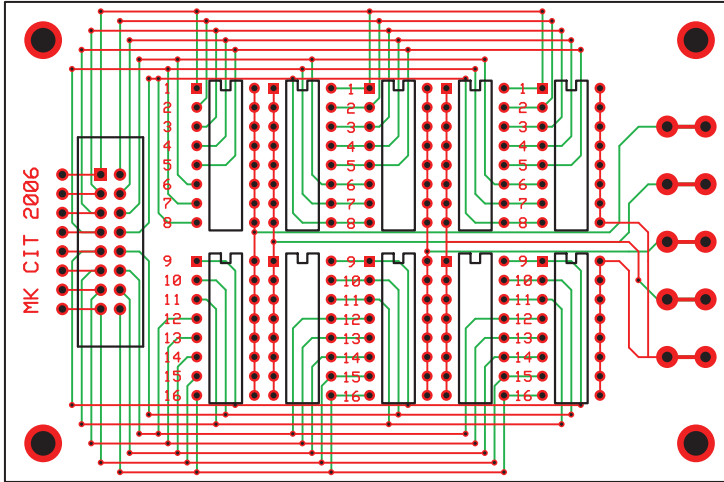
Figure C.3. Printed circuit board layout for SPCM switch box. The circuit connects a 16-pin ribbon-cable header or DIP socket (left) to five terminals (right) using ten 8-position DIP switches (center).

Specimen stage. The microscope system includes a manual x–y translation with $> 1''$ travel, as well as a piezo scan stage with 100 μm of x–y travel. Bolted to the piezo scan stage is a low-profile sample holder that was built to enable microscopy on electrically contacted devices. The sample holder consists of an aluminum back-plate, a printed circuit board, and a 16-pin, zero-insertion-force (ZIF), dual-inline-pin (DIP) socket (3M, P/N 216-6278-00-3303). A 16-conductor ribbon cable connects the sample holder to the switch box located immediately beside the microscope stage.

Switch box. The switch box permits up to five terminals to be connected to the packaged device pins. For each terminal, a bank of DIP switches addresses which pin(s) are connected. A 'grounding' toggle switch is also provided for each terminal, which when closed, shorts the terminal to chassis ground. This provides some protection for loading/unloading of static-sensitive devices, and also provides a convenient way to ground one terminal of the device for short-circuit SPCM measurements. The printed circuit board for the switch box is shown in Figure C.3.

Transimpedance amplifier. The current preamplifier, or *transimpedance amplifier* (TIA), amplifies the specimen current by 10^7 Ω (140 dBΩ) to produce a detectable voltage signal for the lock-in amplifier (LIA). An active TIA enables much faster system response than a shunt resistor alone, and also provides a virtual ground for straightforward device biasing.

A schematic of the TIA is shown in Figure C.4. A low-noise, JFET-input-stage operational amplifier (OPA657, Texas Instruments) was chosen for its high gain-bandwidth product (1.6 GHz) and low input bias current
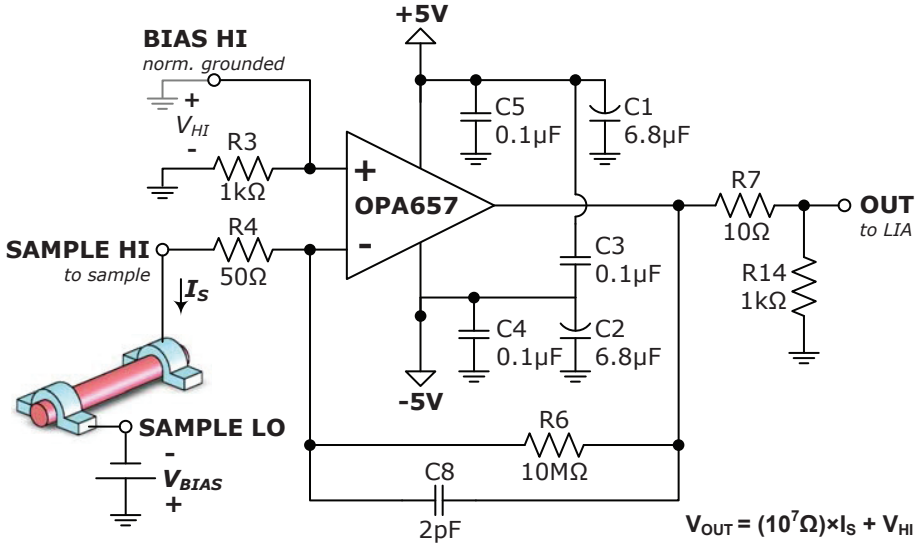
Figure C.4. Transimpedance amplifier circuit schematic.

($<$2 pA). To reduce stray capacitance, the circuit was assembled on a high-speed evaluation board (DEM-OPA-SO-1A, Texas Instruments) using surface-mount components (SO-8 amplifier, 1206 SMD passive components), and was placed in a shielded enclosure. The chosen feedback capacitor value yields good response for single-wire devices and short cable lengths (linear response is observed up to 5 kHz, the maximum chop rate). This is suitable for smaller devices (e.g., 0.1 mm^2 solar cells) but becomes unstable for excessively high input capacitance or cable lengths. Our experience indicates that the practical noise floor for this TIA and specimen configuration (unshielded at room temperature) is ~0.1 pA of specimen photocurrent (using a 1 s time constant for lock-in detection). The TIA approaches saturation for specimen currents in excess of ~0.4 μA (including any dark current or non-chopped photocurrent), although the input stage of our LIA saturates shortly before this point.

Device biasing. The TIA input terminal serves as a virtual ground for the device under test (so long as the amplifier is not saturated). Most SPCM measurements are performed at short circuit (0 V bias) using the switch box to ground the opposite device terminal. If it is desired to bias the device while performing SPCM measurements (e.g., as required for photoconductive devices), the opposite device terminal can instead be connected to a suitable power supply (as shown in Fig. C.4). We typically used a source meter unit (236, Keithley Instruments) to provide specimen bias, which also enabled in situ I–V characterization for specimen currents below ~400 nA.

Lock-in detection and SPCM image formation. A digital lock-in ampli-
fier (SR830, Stanford Research Systems) provides phase-sensitive detection
and filtering of the specimen photocurrent. The analog output channel of
the LIA (0–10 V full scale) is connected to an auxiliary input channel
on the microscope controller.* During confocal (or near-field) microscopy
scans, the microscope software is then configured to record the voltage on
this input channel to form the SPCM image. A scaling factor can be spec-
ified within the software so that SPCM images are reported in terms of
specimen photocurrent magnitude (i_D) rather than the LIA output volt-
age (V_{LIA}). The scaling factor can be calculated from the expression for
the system gain:

$$V_{\text{LIA}} = 4.5 \frac{R_{\text{TIA}}}{V_{\text{sens}}} i_D \tag{C.2}$$

where R_{TIA} is the gain of the transimpedance amplifier ($10^7\ \Omega$) and V_{sens}
is the sensitivity range of the LIA.

Calibrated photodiode. An encapsulated Si photodiode (Advanced Photonix,
P/N PDB-C160SM), mounted in a DIP16 package, can be placed in the
specimen stage to determine the incident beam photocurrent (i_{ph}) prior
to each confocal SPCM session. The responsivity of the photodiode has
been calibrated using our spectral response equipment (its external quan-
tum efficiency is 0.67 at $\lambda = 650$ nm). If the value of $V_{\text{LIA}}(i_{ph})$ is used as
the scaling factor within the microscope software (instead of the system
gain factor), then the resulting SPCM images appear in units of external
quantum efficiency rather than specimen current.

C.2   Operating procedures

The following procedures were followed to perform SPCM measurements on
single-wire devices in this thesis work. These are written to serve as instruc-
tions for future users. Typical conditions and instrument settings are shown in
Table C.1.

Safety: *Proper laser safety protocol must be followed at all times. Particular
attention is required whenever an eyepiece is used with the microscope (in-
stead of or in addition to the video camera). High-power excitation sources
should be turned off or disabled before looking into the microscope, and the
eyepiece(s) should be removed prior to using dangerous illumination levels.*

Sample preparation: Devices are mounted and wire bonded in ceramic DIP16
packages (CSB01652, Spectrum Semiconductor Materials, Inc.). The de-
vice wafers are elevated within the cavity to sit flush with the top surface of
the packages. (Recessed devices cannot be approached by short-working-
distance objectives or NSOM tips.) Low-profile wire bonds are carefully
placed so as not to interfere with contact-mode NSOM measurements (if

---

*The SR830 should usually be configured to display/output "R" on CH1.

desired), as well as to fit within the limited working distance of the higher-power microscope objectives. Oversize devices can be accommodated on custom circuit boards rather than ceramic packages. Alternatively, a small probe stage can be used in place of the DIP socket stage, permitting non-wire-bonded devices to be measured, but precluding the use of high-power objectives or near-field excitation.

Source alignment: The desired laser source is coupled into the microscope via a single-mode optical fiber. A dedicated fiber and fiber coupler are provided for the $\lambda = 650$ nm laser source. A second fiber coupler is available for other sources, requiring the selection of an appropriate single-mode fiber and coupling objective. A handheld fiber optic power meter (PM20A, Thorlabs) is used to maximize the coupling efficiency.

The ends of unused fibers are kept covered at all times because they are easily ruined by dust or scratches. Similar care is taken to protect the microscope objectives.

Specimen loading: The microscope arm is first fully extended (upwards) using the handheld controller ("focus up") or the blue buttons on the microscope controller. The black knob at the base of the handheld controller determines the rate of motion. With the objective(s) rotated to the side, the device is inserted into the ZIF socket and the pins are tightened by rotating the actuator with a flathead screwdriver. The device should be mounted as level as possible, using shims if necessary. The objective is then brought into place and the device is coarsely positioned beneath it using the stage translation knobs. The appropriate pins are then selected by toggling the DIP switches within the switch box, completing the circuit to the transimpedance amplifier and bias source (if used).

Coarse focusing: The field aperture diaphragm is first contracted to ensure that its projection will cast an easily identifiable feature on the device, so that the focal plane can be identified even if no device features are present. The microscope arm is then lowered while monitoring the eyepiece video feed. The image increases in brightness as the focal point is approached,

Table C.1. Typical conditions and instrument settings for SPCM measurements.

Incident beam photocurrent (i_{ph})	100 nA
Chop rate (f)	180 Hz
LIA sensitivity (V_{sens})	1 V
LIA filter settings	Synchronous, $\tau = 1$ ms
Pixel delay time	10 ms
Pixel size	250×250 nm
Acquisition time	3–10 min
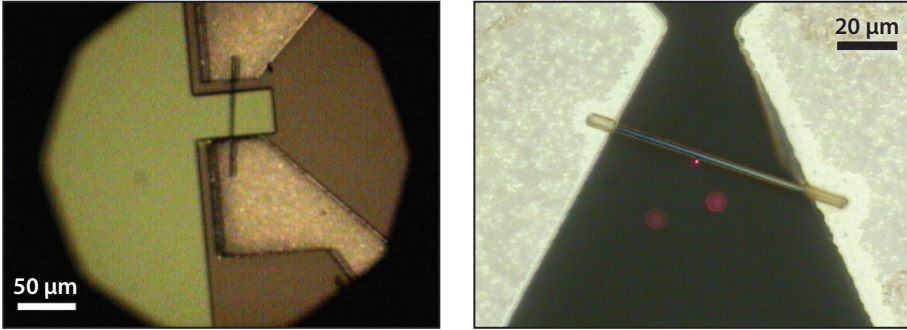
Figure C.5. Confocal SPCM focusing procedures.   **Left**: the field aperture diaphragm is contracted to assist in coarse focusing (20× objective shown). The apparent astigmatism indicates a mild specimen tilt (corrected by shimming the lower left-hand side of the device). **Right**: for fine focusing, the beam is incident immediately adjacent to (but not striking) a single-wire device (50× objective shown). The two defocused beam spots are reflections from internal microscope optics and do not actually strike the specimen.

> converging to an image of the field aperture when focused. The field aperture can then be dilated to provide a larger field of view. The device of interest is located using the stage translation knobs, the microscope arm is re-focused to produce optimal image quality in the eyepiece camera, and then the excitation beam is focused to a minimal apparent spot size using the focusing micrometer on the microscope's fiber input port.

Lock-in configuration: With the beam incident on the device of interest, the illumination intensity and LIA settings are adjusted to produce the desired signal quality. For signals exceeding ~1 mV, the TIA output can be directly monitored on the oscilloscope (using averaging if necessary). The LIA sensitivity range (V_{sens}) is chosen so that illumination of the 'brightest' specimen area produces 40–90% of the full-scale reading. The LIA time constant and filter settings are chosen to yield the fastest response speed that still produces suitable output stability. We targeted an output stability of 1–2% over the course of several seconds, as displayed on the LIA front panel or observed on the oscilloscope. Our experience indicates that the LIA's synchronous filter alone provides suitable noise rejection, permitting arbitrarily short time constants to be used in the normal filter stage.[*]

Fine focusing: The specimen stage is translated so that the laser spot narrowly misses an active device region (i.e., 1–2 μm away from the edge of a metal contact or to either side of a single-microwire device). While monitoring the LIA output channel on the oscilloscope (~1 s per division time

---

[*]This was true so long as the chopper wheel phase jitter was low. A 2-aperture chopper wheel yielded optimal performance in this regard.

base, zooming as necessary) the beam focus knob is then adjusted so as to produce the minimum LIA output value, corresponding to an optimal focusing of the beam into the inactive region of the device. If no minimum is found, the beam is visually re-focused and the procedure is repeated at a slightly different spatial location.

Scan configuration: The x–y piezo scanners are centered ("go to" tab in software) and the device is translated (using the stage knobs) so as to fit within the piezo scan range (indicated by the red square overlaid in the video feed). The scan parameters (width, height, timing, and pixel density) are specified in the microscope control software (first ensuring that the software is in 'confocal' mode). Within the input configuration tab ("ADC" button), the channel corresponding to the LIA output voltage (channel 3) must be selected, specifying the correct scaling factor if desired. The scan speed for SPCM measurements must not exceed the system response speed, which depends on the time constant and filter settings on the LIA. In general, the pixel delay time should be at least 6 times the LIA time constant value (for 24 dB/octave filtering). For synchronous filtering, the pixel delay time should be at least as long as the optical chopping period.

Upon starting each scan, the software automatically activates the APD within the lower microscope assembly. Users should ensure that the APD is protected from stray light sources prior to starting measurements.

Near-field excitation: Near-field SPCM measurements are performed with the microscope configured for NSOM. Briefly, the NSOM tip/objective assembly is installed and the excitation laser is coupled through the tip aperture. The deflection laser and photodiode are aligned and the feedback parameters are configured. The device is then coarsely positioned beneath the tip using the stage translation knobs, then the approach procedure is performed. Once in contact mode, the stage translation knobs should not be used. A coarse topography scan is performed to locate the device. The tip is then placed upon the active device region (using the software "go to" feature) to configure the LIA settings prior to SPCM scans.

C.3   Extended capabilities

The following types of experiments and equipment upgrades have been investigated or proposed in the course of this thesis work.

Excitation sources. As of this writing, the $\lambda = 650$ nm semiconductor diode laser remains the only permanently installed excitation source for SPCM measurements. However, the microscope's fiber-coupled excitation port permits a broad range of potential excitation sources—for example, the $\lambda = 405$ nm laser that was temporarily installed in the course of this thesis work. In 2008, René de Waele et al. established a beam path for the use of a supercontinuum laser (Fianium SC400-series) as either a broadband or

tunable monochromatic excitation source. The supercontinuum laser it-
self is shared between several instruments (including our integrating-sphere
photospectrometer); however, the optics and monochromator remain in-
stalled and available for use with the SPCM instrument. In theory, the
SC400-series supercontinuum lasers provide useful excitation energy from
$\lambda = 400$ nm to beyond 2 μm. In practice, the accessible excitation wave-
lengths are limited by the microscope optics (most of which are optimized
and AR-coated for visible wavelengths) as well as the optical fiber (which
should support a single mode for optimal SPCM imaging). Furthermore,
the microscope includes a series of beamsplitters and filters for the NSOM
tip deflection laser ($\lambda \sim 780$ nm). These must be temporarily removed to
enable near-infrared excitation or collection for confocal-mode SPCM mea-
surements. Because the microscope controller provides front-panel access
to analog signals within the system, a broad variety of experiments can
be envisioned. For example, the "z-height" DAC channel that is normally
connected to the z-axis piezo driver, can instead be connected to a system
that varies the excitation wavelength. In this configuration, instructing
the software to perform a three-dimensional (height-resolved) confocal mi-
croscopy scan will instead collect a series of wavelength-resolved SPCM
scans. We also note that excitation-source instabilities can be corrected
by using an external reference photodetector to monitor the source inten-
sity as a separate image channel. The specimen photocurrent image can be
normalized to the source intensity image within the microscope software.
A similar procedure was used to improve the accuracy of our integrating
sphere photo spectrometer.

Probe stage. The combination of packaged (wire-bonded) devices and the low-
profile DIP-socket SPCM stage provide a robust platform for high-resolution,
low-noise SPCM measurements. However this approach is not feasible for
all types of devices—such as the Si microwire-array solar cells fabricated by
Morgan Putnam et al. (see Figure 6.1), which had fragile ITO top contacts
that were not amenable to wire bonding. To enable SPCM measurements
on these devices, Putnam built a small probe stage that can be affixed
to the piezo scanner in place of the DIP-socket stage. This precludes the
use of high-resolution objectives or NSOM tips, but nonetheless produces
excellent results using a 20× long-working-distance objective. A similar
approach was employed to perform SPCM on micro-pillar solar cells fab-
ricated by Brendan Kayes. [1, § 5.6]

Four-probe biasing. The devices studied in this thesis typically had low con-
tact resistance that could be safely neglected in the analysis of the SPCM
results. However, devices with larger contact resistance or more complex
behavior can, in theory, be characterized by SPCM using a feedback loop to
bias the device using separate source/sense electrodes (analogous to four-
probe $I-V$ measurements). Although such measurements could be per-
formed using the same four-probe source-measure units used for our $I-V$
measurements (Keithley 236), these instruments lack an analog output
channel for direct interconnection to a lock-in amplifier or the microscope

controller's auxiliary input channels. The potentiostat employed in our photoelectrochemical absorption studies (Gamry Reference 600) seems to offer a promising combination of sensitivity, speed, and analog output capabilities. Alternatively, the design of our transimpedance amplifier could be modified to include the device segment enclosed by adjacent source/sense electrodes within its the feedback path; adding a differential voltage sensor across the feedback resistor to determine the specimen current.

Enlarged scan area. The utility of our SPCM instrument is presently limited by the 100×100 μm x–y range of the piezo scanners—requiring many SPCM images to be manually stitched together to study even the small (~0.1 mm^2) microwire-array solar cells fabricated by Putnam et al. Future studies may benefit from a large-area scan stage. We note that this will also necessitate means to null or correct for specimen tilt. In our work it was difficult (but not impossible) to manually align the packaged devices within the focal plane of the microscope, requiring an iterative shimming/refocusing process to obtain suitable alignment over 100 μm length scales. A micrometer-driven tilt stage would likely be required to null specimen tilt over larger scan areas. Alternatively, specimen tilt could be corrected by varying the height of the z piezo stage as a function of x–y scan position. This can be easily accomplished by affixing the appropriate voltage dividers and adders between the analog (x,y) DAC channels and the z piezo driver, or by incorporating a similar correction within the software. A $1'' \times 1''$ scan stage and a controller module that supports tilt correction are offered by WITec.

Optical microscopy. Although the extent of our single-wire devices was directly evident from their SPCM images, the structure of other devices may prove more difficult to correlate with SPCM data. We note that confocal microscopy data can be recorded at the same time as SPCM data by connecting the microscope's APD or suitable photodetector to the reflection-mode confocal collection port. Confocal microscopy will provide substantially higher resolution images than the eyepiece video camera, and will circumvent any spatial mapping errors between the cursor positions on the video camera feed and the SPCM data within the software. Partially transparent devices would also permit transmission-mode confocal or near-field microscopy (with a clear-field stage). For planar devices with specular surfaces, this could (in theory) permit simultaneous measurements of reflection, transmission, and external quantum efficiency; all with the approximate resolution of confocal microscopy.

Bibliography

[1] B. M. Kayes. *Radial pn junction, wire array solar cells.* PhD thesis, California Institute of Technology, **2008**. ⎆

[2] M. C. Putnam. *Si Microwire-Array Solar Cells.* PhD thesis, California Institute of Technology, **2010**.

[3] A. Yeonghwan, J. Dunning, and J. Park. Scanning photocurrent imaging and electronic band studies in silicon nanowire field effect transistors, *Nano Letters*, 5(7):1367–1370, **2005**. ⎆

[4] Y. Gu, J. P. Romankiewicz, J. K. David, J. L. Lensch, L. J. Lauhon, E. S. Kwak, and T. W. Odom. Local photocurrent mapping as a probe of contact effects and charge carrier transport in semiconductor nanowire devices, *Journal of Vacuum Science & Technology, B: Microelectronics Processing and Phenomena*, 24:2172–2177, **2006**. ⎆

[5] J. E. Allen, D. E. Perea, E. R. Hemesath, and L. J. Lauhon. Nonuniform nanowire doping profiles revealed by quantitative scanning photocurrent microscopy, *Advanced Materials*, 21(30):3067–3072, **2009**. ⎆

[6] Y. Gu, J. P. Romankiewicz, and L. J. Lauhon. Quantitative characterization of carrier transport in nanowire photodetectors, *Proceedings of SPIE*, 6479:64790C, **2007**. ⎆

[7] Y. Gu, E. S. Kwak, J. L. Lensch, J. E. Allen, T. W. Odom, and L. J. Lauhon. Near-field scanning photocurrent microscopy of a nanowire photodetector, *Applied Physics Letters*, 87(4):043111, **2005**. ⎆

[8] Y. Gu, J. P. Romankiewicz, J. K. David, J. L. Lensch, and L. J. Lauhon. Quantitative measurement of the electron and hole mobility-lifetime products in semiconductor nanowires, *Nano Letters*, 6(5):948–952, **2006**. ⎆

[9] J. E. Allen, E. R. Hemesath, and L. J. Lauhon. Scanning photocurrent microscopy analysis of Si nanowire field-effect transistors fabricated by surface etching of the channel, *Nano Letters*, 9(5):1903–1908, **2009**. ⎆

[10] J. E. Allen, G. Yi, J. P. Romankiewicz, J. L. Lensch, S. J. May, T. W. Odom, B. W. Wessels, and L. J. Lauhon. Measurement of minority carrier diffusion lengths in semiconductor nanowires. In *IEEE Device Research Conference*, pages 289–290, University Park, PA, USA, 26–28 June 2006, **2006**. IEEE, Piscataway, NJ, USA. ⎆

[11] C. Colombo, M. Heibeta, M. Gratzel, and A. Fontcuberta i Morral. Gallium arsenide p-i-n radial structures for photovoltaic applications, *Applied Physics Letters*, 94(17):173108–3, **2009**. ⏍